Proceeding Series of the Brazilian Society of Computational and Applied Mathematics, v. 11, n. 1, 2025.

Trabalho apresentado no XLIII CNMAC, Centro de Convenções do Armação Resort - Porto de Galinhas - PE, 2024

Proceeding Series of the Brazilian Society of Computational and Applied Mathematics

A Linear Potential Reconstruction Technique Based on Raviart-Thomas Basis Functions for Cell-Centered Finite Volume Approximations to the Darcy Problem

Jhabriel Varela[1], Christian E. Schaerer[2]
Polytechnic School, National University of Asunción, Paraguay
Eirik Keilegavlen[3]
Center for Modeling of Coupled Subsurface Dynamics, Department of Mathematics, University of Bergen, Norway

Abstract. We propose a technique to recover linear potentials from the solution obtained from cell-centered finite volume approximations to the scalar elliptic problem, i.e., the cell-centered potentials and the normal fluxes on the edges. The technique employs lowest-order Raviart-Thomas basis functions to compute a local potential gradient, which is then used to obtain nodal potentials and from there a global energy-conforming potential. Numerical convergence tests in two dimensions show that the gradient of the reconstructed potential converges at $\mathcal{O}(h)$, outperforming reconstructions obtained via averaging of cell-centered values and producing similar results compared to a quadratic reconstruction technique.

Keywords. potential reconstruction, gradient reconstruction, error estimation, lowest-order Raviart-Thomas basis functions

1 Introduction

The cell-centered finite volume method (CCFVM) is the industry standard in computational fluid dynamics and reservoir engineering simulations. Regardless of the specific application, one often wishes to estimate numerical errors to employ them as part of adaptive mesh coarsening/refinement workflows, as this results in considerable computational savings. Estimating errors using *a posteriori* techniques typically requires computing the gradient of the primary variable, i.e., the fluid potential, temperature, concentration, etc. Unfortunately, for lowest-order CCFVM, since the potential is only constant in each cell, this is not possible, and one must enhance its regularity to produce at least a linear potential. Depending on the context, this process is referred to as *potential reconstruction* or *gradient reconstruction*.

Several techniques of different complexity and accuracy have been proposed. The reader coming from the computational fluid dynamics community may be familiar with techniques based on the Green-Gauss theorem (GG methods) or the least-squares approach (LSQ methods) [7, 10, 13], whereas the reader coming from the *a posteriori* error analysis community might recognize the simple patch-wise average of cell-centered potentials [3] or the more elaborate schemes proposed by Vohralík [11, 12] and coauthors.

In this contribution, we propose a linear potential reconstruction technique that employs the available CCFVM flux information but does not require solving an auxiliary problem or performing

[1]jhabriel@pol.una.py
[2]cschaer@pol.una.py
[3]eirik.keilegavlen@uib.no

numerical integration. As demonstrated by the numerical tests, the proposed potential reconstruction technique converges at $\mathcal{O}(h)$, resulting in a competitive alternative that can be used as part of error estimation routines. The rest of the paper is organized as follows: In the following section, we introduce the model problem and its CCFVM approximation. In Section 3, we introduce the proposed technique and other well-established alternatives. Finally, in Section 4 we perform the numerical tests, and in Section 5 we draw our conclusions.

2 Model and Finite Volume Discretization

In this section, we introduce the model problem and its CCFVM discretization. For the sake of compactness, we limit our exposition and analysis to two dimensions. However, the extension to three dimensions is straightforward and does not require any special consideration.

2.1 The Model Problem

Let $\Omega \subset \mathbb{R}^2$ be an open and bounded domain with a smooth boundary $\Gamma \subset \mathbb{R}$. The Darcy problem in strong dual form is given by

$$\nabla \cdot \mathbf{u} = f, \qquad \text{in}\,\Omega, \tag{1a}$$

$$\mathbf{u} = -\mathbb{K}\nabla p, \qquad \text{in}\,\Omega, \tag{1b}$$

$$p = g_\Gamma, \qquad \text{on}\,\Gamma, \tag{1c}$$

where $\mathbf{u}$ is the Darcy flux, $f \in L^2(\Omega)$ is a source term, $\mathbb{K}$ is the symmetric positive-definite 2×2 permeability matrix[4] with diagonal components K_{xx} and K_{yy} and off-diagonal components K_{xy}, p is the potential and $g_\Gamma \in H^{1/2}(\Gamma)$ is a prescribed Dirichlet function on the boundary Γ. Moreover, we define $g \in H^1(\Omega)$ as a function satisfying $g_\Gamma = g|_\Gamma$ in the sense of traces.

2.2 Cell-Centered Finite Volume Approximation

Let $\mathcal{T}_h$ be a shape-regular simplicial partition of the domain Ω, such that $\overline{\Omega} = \cup_{K \in \mathcal{T}_h} K$ with K denoting a two-dimensional simplex, i.e., a triangle. A CCFVM scheme is based on integrating (1a) locally and then applying the Gauss theorem to obtain [8]

$$(\nabla \cdot \mathbf{u}, 1)_K = (\mathbf{u} \cdot \mathbf{n}, 1)_{\partial K} = \sum_{e \in \mathcal{E}_K} (\mathbf{u} \cdot \mathbf{n}|_e, 1)_e = \sum_{e \in \mathcal{E}_K} (u_e, 1)_e = (f, 1)_K, \qquad \forall\, K \in \mathcal{T}_h, \tag{2}$$

where u_e is the exact normal flux on the edge e, associated with the set of edges $\mathcal{E}_K$ of the simplex K. Here, and in the following, we use $(\cdot, \cdot)_S$ to denote the L_2 inner product on the domain S.

The normal fluxes are now related to their neighboring cell-centered potentials $p_{h,K}$ via the discrete version of (1b)

$$(u_e, 1)_e \approx (u_{h,e}, 1)_e = \sum_{K \in \mathcal{F}_e} T_{K,e}\, p_{h,K}, \quad \forall\, e \in \mathcal{E}_K, \quad \forall\, K \in \mathcal{T}_h, \tag{3}$$

where $\mathcal{F}_e$ denotes the set of neighboring cells of the edge e and $T_{K,e}$ are transmissibility coefficients. The definition of $T_{K,e}$ depends on the CCFVM scheme employed and the type of grid. For this paper, the precise expression for $T_{K,e}$ is not relevant. The interested reader, however, is referred to [1] for an excellent exposition.

[4] We emphasize that the permeability matrix $\mathbb{K}$ can be both anisotropic *and* heterogeneous.

DOI: 10.5540/03.2025.011.01.0332

Equations (2) and (3) allow us to write a system of linear algebraic equations that can be solved to obtain cell-centered potentials $p_{h,K} \in \mathbb{P}_0(K)$ for all $K \in \mathcal{T}_h$ and (upon post-processing) face-centered normal fluxes $u_e \in \mathbb{P}_0(e)$ in all $e \in \mathcal{E}_K$ for all $K \in \mathcal{T}_h$. For the numerical examples in Section 4, we shall employ the Multi-Point Flux Approximation (MPFA-O) scheme, see also [1, 8].

3 Potential Reconstruction

As we have mentioned in the introduction, computing energy norms typically require calculating the gradients of the approximated potentials. We thus need to enhance the regularity of the CCFVM potential using some interpolant of the type $\mathcal{G}_k : \mathbb{P}_0(\mathcal{T}_h) \to \mathbb{P}_k(\mathcal{T}_h) \cap H_0^1(\Omega) + g$, for some $k \in \mathbb{N}_{>0}$, where $H_0^1(\Omega)$ is the energy space with vanishing traces on the boundaries and $\mathbb{P}_k(\mathcal{T}_h) : \{q \in L^2(\Omega) : q \in \mathbb{P}_k(K) \ \forall \ K \in \mathcal{T}_h\}$ is the broken space of polynomial functions.

3.1 A Lowest-Order Raviart-Thomas-Based Reconstruction

In the following, we present the steps to obtain the reconstructed potential starting from a CCFVM solution. To keep the computational cost low, the proposed reconstruction technique seeks an interpolant $\mathcal{G}_1$. We shall refer our scheme to as `P1-RT0-BASED`.

Step 1: Extension of Normal Fluxes Into the Interior of the Elements

Having available the normal fluxes $u_{h,e}$ on each edge, the first step is to extend them onto the interior of each $K \in \mathcal{T}_h$ to obtain a local velocity $\mathbf{v}|_K$. This can be achieved using lowest-order Raviart-Thomas basis functions $\mathbb{RT}_0(K) : [\mathbb{P}_0(K)]^2 + \mathbf{x}\mathbb{P}_0(K)$. In two dimensions, the vector $\mathbf{v}|_K \in \mathbb{RT}_0(K)$ is fully-determined by three constants a_K, b_K and c_K such that

$$\mathbf{v}|_K = \begin{pmatrix} a_K x + b_K \\ a_K y + c_K \end{pmatrix}, \qquad \forall \ K \in \mathcal{T}_h. \tag{4}$$

For the details, we refer to [2]. We remark that this step should not represent an additional cost to the *a posteriori* analysis, since the global Darcy flux $\mathbf{v} \in \mathbf{H}(\mathrm{div}, \Omega)$ is typically required independently of the potential reconstruction technique employed.

Step 2: Computation of Potential Gradients

Using Darcy's law (1b), we can now obtain a vector quantity

$$\mathbf{r}|_K = -\mathbb{K}^{-1}\mathbf{v}|_K, \qquad \forall \ K \in \mathcal{T}_h, \tag{5}$$

that approximates a local potential gradient. Since the permeability matrix is defined locally in each $K \in \mathcal{T}_h$, computing its inverse has a negligible cost.

Step 3: Computation of Nodal Potentials

Let V denote a node (vertex) from the set of nodes $\mathcal{V}_K$ of K and B_K the barycenter of the cell K. For all interior nodes, we can now compute a nodal potential $\tilde{s}(V)$ by adding the CCFVM potential to the projected local potential gradient

$$\tilde{s}(V) = p_{h,K} + [\mathbf{x}(V) - \mathbf{x}(B_K)] \cdot \mathbf{r}|_K(B_K), \qquad \forall \ V \in \mathcal{V}_K, \quad \forall \ K \in \mathcal{T}_h. \tag{6}$$

DOI: 10.5540/03.2025.011.01.0332

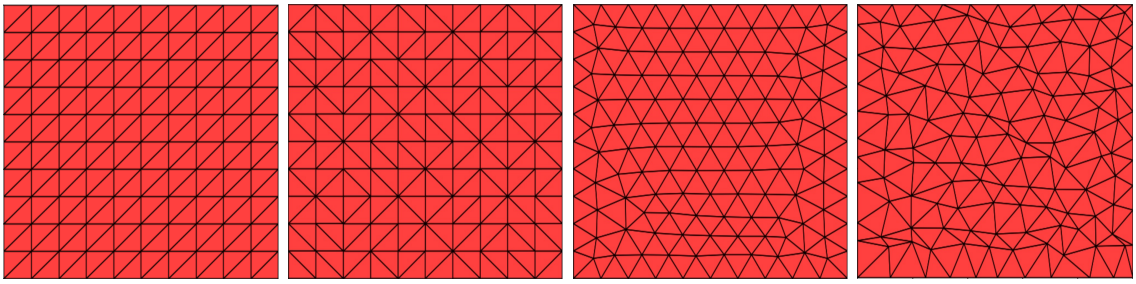

Figure 1: Triangulations of the unit square employed in the numerical tests. (a) Regular structured. (b) Irregular structured. (c) Unstructured. (d) Perturbed unstructured. Source: Authors.

Step 4: Application of the Oswald Interpolator

The nodal potentials obtained in Step 3 are in general non-conforming, in the sense that for two simplices K and K' sharing a common node V, the values of $\tilde{s}(V)$ do not necessarily match. The remedy is to employ the so-called Oswald interpolator [4], which takes the average of $\tilde{s}(V)$ sharing common Lagrangian nodes. We therefore seek for $s(V)$ such that

$$s(V) = \begin{cases} \frac{1}{|\mathcal{P}_V|} \sum_{K \in \mathcal{P}_V} \tilde{s}(V), & V \text{ is an interior node} \\ g_D(V), & V \text{ is a boundary node} \end{cases} \tag{7}$$

where $|\mathcal{P}_V|$ refers to the cardinality of the set $\mathcal{P}_V$ and g_Γ is assumed to be continuous on Γ.

3.2 Alternative Reconstruction Schemes

Is clear that the construction of $\mathcal{G}_k$ is not unique. Here, we present two other well-established techniques to construct $\mathcal{G}_1$ and $\mathcal{G}_2$. The first [3] takes the volume-weighted average of cell-centered potential over node patches, whereas the second [11, 12] solves a local Darcy problem with mean value potential preservation and then applies the Oswald interpolator.

3.2.1 Reconstruction via Averaging of Cell-Centered Potentials

Let $p_h \in \mathbb{P}_0(K)$ be available for all $K \in \mathcal{T}_h$. Then, a simple way to obtain nodal potential values is to take the (weighted) average of cell-centered potentials over patches [3]:

$$s(V) = \begin{cases} \dfrac{\sum_{K \in \mathcal{P}_V} |K| \; p_{h,K}}{\sum_{K \in \mathcal{P}_V} |K|}, & V \text{ is an interior node} \\ g_D(V), & V \text{ is a boundary node} \end{cases} \tag{8}$$

where $|K|$ is the Lebesgue measure of the simplex K, i.e., the area of the triangle. Since this technique produces unique values at the nodes, the resulting potential is already energy-conforming. We shall refer to this scheme as `P1-CC-AVG`.

3.2.2 A Quadratic Potential Reconstruction

As part of a formal primal formulation-based *a posteriori* error analysis in the context of mixed finite element methods, Vohralík [11, 12] proposed the following post-processing of the cell-centered potentials: Let $p_{h,K} \in \mathbb{P}_0(K)$ and $\mathbf{v}_h|_K \in \mathbb{RT}_0(K)$ be available for all $K \in \mathcal{T}_h$. Then, for

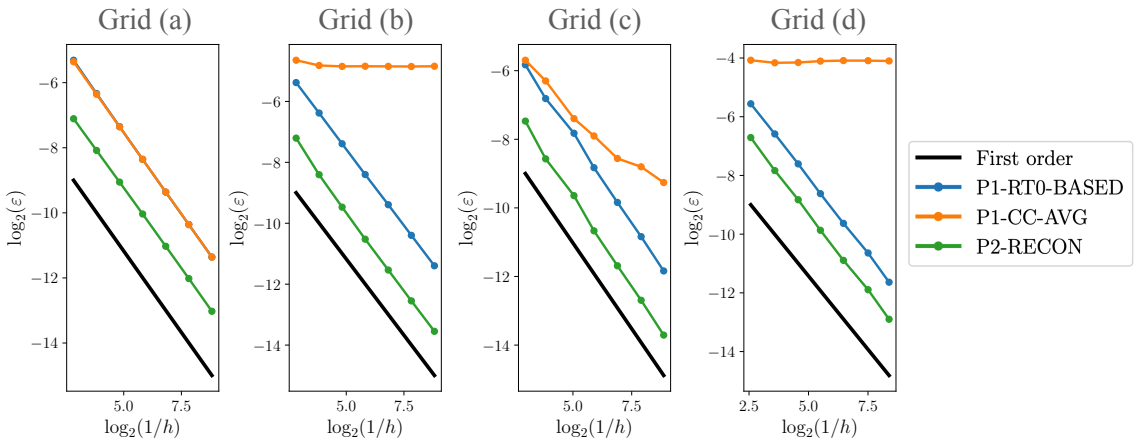

Figure 2: Convergence analysis for a parabolic potential profile with unit permeability. The grid types (a), (b), (c), and (d) correspond to those from Figure 1. Source: Authors.

all $K \in \mathcal{T}_h$, find $\tilde{s} \in \mathbb{P}_2(K)$ such that

$$-\mathbb{K}\nabla\tilde{s}|_K = \mathbf{v}|_K, \tag{9a}$$

$$\frac{1}{|K|}(\tilde{s}|_K, 1)_K = p_{h,K}. \tag{9b}$$

When $\mathbb{K}$ is a dense tensor, $\tilde{s}|_K$ is a full quadratic polynomial in each cell. Furthermore, since $\tilde{s}|_K \in \mathbb{P}_2(K)$ results in a globally non-conforming potential, we apply the Oswald interpolator to obtain $s \in \mathbb{P}_2(\mathcal{T}_h) \cap H_0^1(\Omega) + g$ (c.f., Step 4 from Sec. 3.1). An important point to remark is that the interpolation must be performed in all Lagrangian nodes (not only in the physical mesh nodes) since the potential is now quadratic in each element. We shall refer to this scheme as `P2-RECON`.

4 Numerical Tests

To test the reconstruction techniques `P1-RT0-BASED`, `P1-CC-AVG`, and `P2-RECON`, we shall employ four triangular grids as shown in Figure 1. For each type of grid, we perform two numerical convergence tests using the method of manufactured solutions [9]. The first assumes a parabolic potential profile $p(x, y) = x(1 - x)y(1 - y)$ with unit permeability and the second assumes a trigonometric potential profile $p(x, y) = \cos(2\pi x)\cos(2\pi y)$ with $K_{xx} = 7.7500$, $K_{yy} = 3.2500$ and $K_{xy} = 3.8971$ as employed in [6]. Boundary conditions are imposed such that they satisfy the exact potential on Γ. To measure the errors, we compute the difference between the exact and reconstructed potential gradients, with the error defined as $\varepsilon := \left(\sum_{K\in\mathcal{T}_h} \|\nabla p - \nabla s)\|_K^2\right)^{1/2}$.

For each convergence analysis, we employ seven levels of successively refined mesh sizes h, i.e., 0.1, 0.05, 0.025, 0.00125, 0.00625, 0.003125, and 0.0015625. The numerical tests are implemented using the Python library `PorePy` [5] and are openly available[5] for reproduction.

4.1 Analysis of Results

Convergence plots for the first and second set of experiments are shown respectively in Figures 2 and 3. Analyzing the results, we can see that `P1-CC-AVG` converges only for the case of struc-

[5] `www.github.com/jhabriel/potential_reconstruction.git`

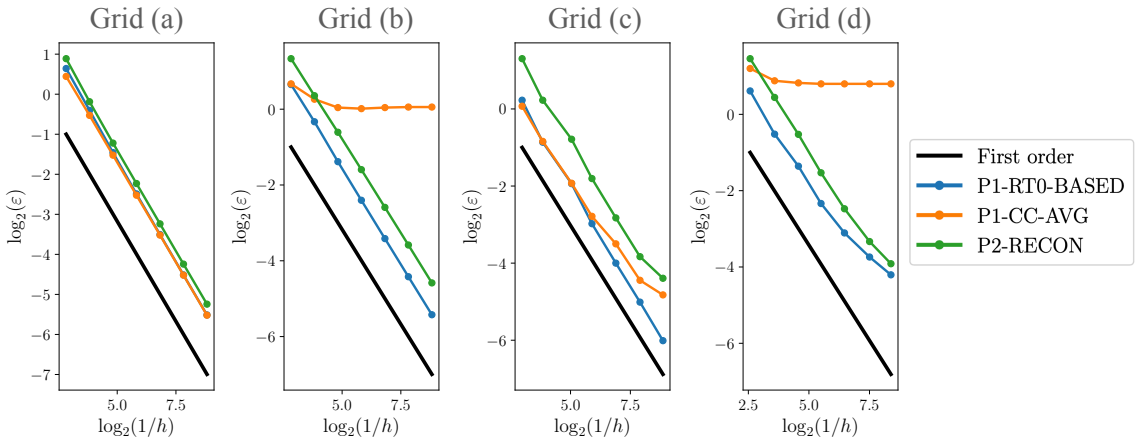

Figure 3: Convergence analysis for a trigonometric potential profile with anisotropy. The grid types (a), (b), (c), and (d) correspond to those from Figure 1. Source: Authors.

tured regular grids. In the case of unstructured grids, the convergence comes with some accuracy degradation. Furthermore, for structured irregular and perturbed unstructured grids, the scheme is, in fact, zero-order convergent. A similar behavior was reported in [7, 10]. Later, in [13], it was proved that this occurs when the face midpoint of an element does not divide the segment connecting the centers of its two adjacent cells equally. This results in the reconstructed potential to converge only at $\mathcal{O}(h)$ and consequently its gradient at $\mathcal{O}(1)$.

The quadratic reconstruction technique `P2-RECON` converges at $\mathcal{O}(h)$ in all cases, except for the trigonometric potential from Figure 3 with unstructured and perturbed unstructured grids, where a mild lost in the convergence rates can be seen at highly refined mesh sizes. This behavior could be linked to the presence of anisotropy and deserves further investigation.

Finally, the proposed technique `P1-RT0-BASED` seems to converge at $\mathcal{O}(h)$ in almost all scenarios. Notably, the method seems stable for the case of unstructured grids while sharing similar difficulties as `P2-RECON` when the nodes are perturbed.

5 Conclusion

In this article, we have proposed a technique to recover a linear potential from the solutions obtained with cell-centered finite volume methods. The technique is simple to implement and does not require numerical integration. Numerical examples carried on four different triangular grids and for two different manufactured solutions (one including anisotropy) suggest that potential gradients converge at $\mathcal{O}(h)$. Based on our numerical investigations, unless the grid employed is structured and regular, we do not recommend employing the technique based on averaging cell-centered potentials.

Acknowledgments

JV was funded by the Paraguayan National Council of Science and Technology (CONACYT) through the program Advanced Human Capital Insertion in Academia PRIA01-8. C.E.S. acknowledges FEEI-CONACYT-PRONII.

References

[1] I. Aavatsmark. "An introduction to multipoint flux approximations for quadrilateral grids". In: **Computational Geosciences** 6.3-4 (2002). Locally conservative numerical methods for flow in porous media, pp. 405–432. ISSN: 1420-0597. DOI: 10.1023/A:1021291114475.

[2] C. Bahriawati and C. Carstensen. "Three MATLAB implementations of the lowest-order Raviart-Thomas MFEM with a posteriori error control". In: **Computational Methods in Applied Mathematics** 5.4 (2005), pp. 333–361. DOI: 10.2478/cmam-2005-0016.

[3] S. Cochez-Dhondt, S. Nicaise, and S. I. Repin. "A posteriori error estimates for finite volume approximations". In: **Mathematical Modelling of Natural Phenomena** 4.1 (2009), pp. 106–122. ISSN: 0973-5348. DOI: 10.1051/mmnp/20094105.

[4] O. A. Karakashian and F. Pascal. "A Posteriori Error Estimates for a Discontinuous Galerkin Approximation of Second-Order Elliptic Problems". In: **SIAM Journal on Numerical Analysis** 41.6 (2003), pp. 2374–2399. DOI: 10.1137/S0036142902405217.

[5] E. Keilegavlen, R. Berge, A. Fumagalli, M. Starnoni, I. Stefansson, J. Varela, and I. Berre. "PorePy: An open-source software for simulation of multiphysics processes in fractured porous media". In: **Computational Geosciences** 25.1 (2021), pp. 243–265. DOI: 10.1007/s10596-020-10002-5.

[6] R. A. Klausen and R. Winther. "Robust convergence of multi point flux approximation on rough grids". In: **Numerische Mathematik** 104 (2006), pp. 317–337. DOI: 10.1007/s00211-006-0023-4.

[7] D. Mavriplis. "Revisiting the least-squares procedure for gradient reconstruction on unstructured meshes". In: **16th AIAA Computational Fluid Dynamics Conference**. 2003, p. 3986.

[8] J. M. Nordbotten and E. Keilegavlen. "An Introduction to Multi-point Flux (MPFA) and Stress (MPSA) Finite Volume Methods for Thermo-poroelasticity". In: **Polyhedral Methods in Geosciences**. Ed. by Daniele Antonio Di Pietro, Luca Formaggia, and Roland Masson. Cham: Springer International Publishing, 2021, pp. 119–158. ISBN: 978-3-030-69363-3. DOI: 10.1007/978-3-030-69363-3_4.

[9] C. J. Roy. "Review of code and solution verification procedures for computational simulation". In: **Journal of Computational Physics** 205.1 (2005), pp. 131–156. DOI: 10.1016/j.jcp.2004.10.036.

[10] E. Sozer, C. Brehm, and C. C. Kiris. "Gradient calculation methods on arbitrary polyhedral unstructured meshes for cell-centered CFD solvers". In: **52nd Aerospace Sciences Meeting**. 2014, p. 1440.

[11] M. Vohralík. "A posteriori error estimates for lowest-order mixed finite element discretizations of convection-diffusion-reaction equations". In: **SIAM Jounral on Numerical Analysis** 45.4 (2007), pp. 1570–1599. ISSN: 0036-1429. DOI: 10.1137/060653184.

[12] M. Vohralík. "Unified primal formulation-based a priori and a posteriori error analysis of mixed finite element methods". In: **Mathematics of Computation** 79.272 (2010), pp. 2001–2032. ISSN: 0025-5718. DOI: 10.1090/S0025-5718-2010-02375-0.

[13] N. Wang, M. Li, R. Ma, and L. Zhang. "Accuracy analysis of gradient reconstruction on isotropic unstructured meshes and its effects on inviscid flow simulation". In: **Advances in Aerodynamics** 1 (2019), pp. 1–31. DOI: 10.1186/s42774-019-0020-9.

